SYNAPTOTAGMIN-9 IN MOUSE RETINA

Chris S. Mesnard [1,2],* Cassandra L. Hays [1,4], Barta, Cody L[1], Gurumurthy CB[3], Thoreson, Wallace B[1,2]

[1]Truhlsen Eye Institute and Department of Ophthalmology and Visual Sciences, [2]Pharmacology and Experimental Neuroscience, [3]Genetics, Cell Biology and Anatomy, University of Nebraska Medical Center, Omaha, NE 68106, USA,

[4]Department of Medical Education, Creighton University, Omaha, NE 68178

Corresponding author: Wallace B. Thoreson, PhD.

Truhlsen Eye Institute
University of Nebraska Medical Center
Omaha, NE 68198-5840

Email: wbthores@unmc.edu

Phone: 402-559-4276

Short title: Synaptotagmin-9 in mouse retina.

7 figures, 18 pages

Abstract

Synaptotagmin-9 (Syt9) is a Ca^{2+} sensor mediating fast synaptic release expressed in many parts of the brain. The presence and role of Syt9 in retina is unknown. We found evidence for Syt9 expression throughout the retina and created mice to conditionally eliminate Syt9 in a cre-dependent manner. We crossed $Syt9^{fl/fl}$ mice with Rho-iCre, HRGP-Cre, and CMV-cre mice to generate mice in which Syt9 was eliminated from rods ($rod^{Syt9CKO}$), cones ($cone^{Syt9CKO}$), or whole animals (CMV^{Syt9}). CMV^{Syt9} mice showed an increase in scotopic electroretinogram (ERG) b-waves evoked by bright flashes with no change in a-waves. Cone-driven photopic ERG b-waves were not significantly different in CMV^{Syt9} knockout mice and selective elimination of Syt9 from cones had no effect on ERGs. However, selective elimination from rods decreased scotopic and photopic b-waves as well as oscillatory potentials. These changes occurred only with bright flashes where cone responses contribute. Synaptic release was measured in individual rods by recording anion currents activated by glutamate binding to presynaptic glutamate transporters. Loss of Syt9 from rods had no effect on spontaneous or depolarization-evoked release. Our data show that Syt9 is acts at multiple sites in the retina and suggest that it may play a role in regulating transmission of cone signals by rods.

Key words: Synaptotagmin, electroretinogram, rod photoreceptor cell, retina

Introduction

Synaptotagmins are a family of Ca^{2+}-sensing proteins that facilitate synaptic exocytosis. Synaptotagmins -1, -2, and -9 serve as Ca^{2+} sensors that trigger fast synchronous release in CNS neurons (Geppert et al., 1994; Pang et al., 2006; Xu et al., 2007). The less-studied Synaptotagmin-9 (Syt9) shares considerable sequence homology with Syt1 and Syt2 (Rickman et al., 2004). Due to a nomenclature issue in the earlier literature, Syt9 was sometimes referred to as Syt5 and vice versa (Fukuda and Sagi-Eisenberg, 2008), so one must use care when reviewing the literature. For these experiments, we used Syt9 NCBI gene ID 60510 (491 amino acids). In the brain, Syt9 is expressed primarily in the hypothalamus, accumbens, striatum, and olfactory bulb (Mittelsteadt et al., 2009; Xu et al., 2007)(http://mouse.brain-map.org). Syt9 has been found to mediate fast, synchronous release in these areas, though with slower kinetics than Syt1 or Syt2 (Kochubey et al., 2016; Xu et al., 2007), along with a lower Ca^{2+} affinity (Hui et al., 2005). Eliminating Syt9 from striatal neurons was found to abolish fast synchronous release of GABA (Xu et al., 2007) but a more recent study in cultured neurons (hippocampal, cortical, and striatal) found that deletion of Syt9 had no effect on evoked inhibitory currents, while loss of Syt1 abolished evoked release in all three neuronal types (Seibert et al., 2022). However, in Syt1 KO neurons, overexpressing Syt9 to levels to match Syt1 expression (~25-fold) was able to rescue loss of synchronous release. Elimination of Syt9 in cultured striatal neurons also resulted in lower spontaneous release of GABA (Seibert et al., 2022). Syt9 is present on both small synaptic and large dense core vesicles (DCVs) of the mouse brain (Fukuda, 2006), and has been found to regulate catecholamine secretion (along with Syt1) from DCVs in cultured PC12 cells (Fukuda et al., 2002; Lynch and Martin, 2007). In the gonadotrophs of female mice, Syt9 has been shown to regulate the release of follicle-stimulating hormone (FSH) from dense core vesicles (Roper et al., 2015).

Nothing is known about possible roles of Syt9 in retina. Consistent with evidence for Syt9 genes in zebrafish retina (Henry et al., 2022), we show evidence for Syt9 in multiple retinal neurons. Selective

elimination of Syt9 from rods caused a reduction in scotopic b-waves and oscillatory potentials, while global elimination of Syt9 increased b-waves, suggesting actions at multiple sites in the retina.

Materials and methods

Mice

Control C57Bl6J and mutant mice aged 4–8 weeks were used for these experiments. Creation of HRGP-Cre and Rho-iCre mice have been described previously (Le et al., 2004; Li et al., 2005). Creation of Syt9^{fl} mice are described elsewhere (Quadros et al., 2017). Syt9^{fl} mice were originally created using C57Bl6N mice and subsequently back-crossed to C7Bl6J mice. Yun Le (Univ. of Oklahoma) generously provided HRGP-Cre mice. Rho-iCre mice were obtained from Jackson Laboratories, Bar Harbor, ME (B6.Cg-Pde6b+ Tg(Rho-iCre)1Ck/Boc; RRID: 015850). Rho-iCre and HRGP-Cre mice selectively express cre-recombinase in rods and cones, respectively (Jin et al., 2020; Le et al., 2004; Li et al., 2005).

Euthanasia was conducted in accordance with AVMA Guidelines for the Euthanasia of Animals by CO2 asphyxiation followed by cervical dislocation. Animal care and handling protocols were approved by the University of Nebraska Medical Center Institutional Animal Care and Use Committee.

Immunohistochemistry

For immunohistochemical experiments, eyes were enucleated after euthanizing the mouse and then placed in oxygenated Ames' medium. After removing the cornea and lens, the posterior eyecup was fixed in 4% paraformaldehyde for 45 min. The eyecup was then washed in PBS 3 times for 10 min each, and cryoprotected in 30% sucrose overnight at 4°C. Eyecups were embedded in OCT compound (Sakura Finetek USA, Torrance, CA) and stored at −80 °C until sectioning at 25 µm with a cryostat (Leica CM 1800; Chicago, IL). Retinal sections were treated with a blocking solution of 1% Triton X-100 and 6% donkey or goat serum (Jackson Immunoresearch, West Grove, PA and Life Technologies, Carlsbad, CA, respectively) for 3 h before applying the primary antibody. The blocking serum was chosen to match the species in

which the secondary antibody was raised. Primary and secondary antibodies were diluted to working concentrations in blocking solution. Sections were incubated in primary antibody at 4 °C overnight and in secondary antibody at room temperature for 2–3 h. Retinal sections were mounted with Vectashield (Vector Labs, Burlingame CA, RRID: AB_2336787) before imaging.

Confocal imaging was performed using NIS Elements software (Nikon, RRID:SCR_014329) and a spinning disk confocal microscope that consisted of a laser confocal scanhead (PerkinElmer Ultraview LCI, Waltham, MA) equipped with a cooled CCD camera (Hamamatsu Orca ER; Hamamatsu City, Shizuoka, RRID:SCR_017105) mounted on a Nikon E600FN microscope. Fluorescent excitation was delivered from an argon/krypton laser at 488, 568 or 648 nm and emission was collected at 525, 607 and 700 nm, respectively. Filters were controlled using a Sutter Lambda 10–2 filter wheel and controller. The objective (water immersion, 60×, 1.2 NA) was controlled with an E662 z-axis controller (Physik Instrumente; Karlruhe, Germany). Image brightness and contrast were adjusted using Nikon Elements, Fiji, and/or Adobe Photoshop software.

Statistical analysis

Statistical analysis and data visualization were done using ClampFit 10 and GraphPad Prism 9 software. Roughly equal numbers of male and female mice were used for these experiments. For ERG measurements, we analyzed the sample for each condition using Dunnett's multiple comparisons test with one-way ANOVA. For comparing spontaneous release rates, we used nested t-tests to compare samples from cells where multiple measurements were made. Data values in the text are reported as mean ± SD. Errors bars for whole cell measurements show 95% confidence intervals.

RNAscope

Eyes were fixed in 10% neutral buffered formalin for 48 h, transferred to 70% ethanol, and processed for paraffin embedding. Five µm thick retina slices were dehydrated at 60°C, deparaffinized and rehydrated in a series of xylene and graded ethanol (100%, 95%, 75%, 50%, dPBS). Slides were rinsed with Dulbecco's phophate-buffered saline (DPBS) and blocked for endogenous peroxidases using 3% H_2O_2 in methanol. Slides were then again rinsed in DPBS. Heat-induced antigen retrieval was completed by submerging sections in 0.1 M sodium citrate, pH 6.39 and heated in a steam chamber at 95°C. The sections were blocked in dPBS with 2.5% normal horse serum for 30 min at room temperature. The following day, after washes in dPBS, secondary ImmPress – HRP Horse Anti-Rabbit IgG Polymer (Vector Laboratories, Burlingame, CA) was applied for 1 h at room temperature.

In situ hybridization for Syt9 RNA was performed using RNAscope with probes targeting Syt9 (Advanced Cell Diagnostics, Newark, CA; Lot #: 20293B). Target amplification and color development was done using the 2.5 HD RED Assay (Advanced Cell Diagnostics, Newark, CA). Visualization was achieved utilizing Nova Red and sections were counterstained with Hematoxylin QS (both from Vector Laboratories, Burlingame, CA).

Electroretinography

ERGs were recorded in vivo using a UTAS Sunburst ganzfeld illuminator (LKC, Gaithersburg, MD, LKC-UTAS-SB). Mice were dark-adapted for ∼12 h prior to experiments and then anaesthetized via intra-peritoneal injection with a ketamine/xylazine drug cocktail (100 mg/kg ketamine, 10 mg/kg xylazine). Core temperature of the mouse was maintained at 37 °C with a heat pad. Tropicamide and proparacaine ophthalmic solution (0.5%) were administered topically to the left eye before the mouse was secured to the platform and a silver/silver chloride wire ring recording electrode was centered on the left cornea. Subcutaneous ground and reference electrodes were placed at the base of the tail and under the scalp, respectively. ERG a-waves provide a measure of photoreceptor responses and were measured from

baseline to the bottom of the downward going negative potential. ERG b-waves reflect responses of second-order ON-type bipolar cells and were measured from the trough of the initial negative deflection of the a-wave to the peak of the positive-going b-wave. Measurements in dark-adapted (scotopic) conditions involved flashes of increasing intensity: 51 dB, −45 dB, −39 dB, −33 dB, −27 dB, −21 dB, −15 dB, −9 dB, −3 dB, and +5 dB. Ten flashes were presented at each intensity, separated by 10 s for steps 1–9 and 20 s between flashes at the highest intensity. Light-adapted (photopic) protocols were performed after background adaptation for 10 min with green light (40 cd/m2) and conducted with the same background. We tested 6 intensities (−6, −3, 0, 4, 7, and 13 dB) with 25 flashes at each intensity separated by 3 s. Oscillatory potentials were extracted from flash ERGs by bandpass filtering the entire trace to remove frequency components below 70 Hz and above 280 Hz using an 8-pole Bessel filter in Clampfit (Axon Instruments, Molecular Devices).

Whole cell recordings

Whole cell recordings from rods were performed using a flatmount preparation of isolated retina. An eye was enucleated immediately after euthanizing the mouse and placed in Ames' medium (US Biological; RRID:SCR_013653) bubbled with 95% O_2/5% CO_2. The cornea was punctured with a scalpel and the anterior segment removed. The retina was isolated by cutting optic nerve attachments. After making four fine cuts at opposite poles, the retina was flattened onto a glass slide in the perfusion chamber with photoreceptors facing up. The retina was anchored in place with a brain slice harp (Warner Instruments, cat. no. 64-0250). The perfusion chamber was placed on an upright fixed-stage microscope (Nikon E600FN) with a 60x water-immersion, long-working distance objective (1.0 NA). Flatmount preparations were superfused with room temperature Ames solution bubbled with 95%/5%CO2 at ~1 mL /min. Outer segments were removed by gentle suction using a patch pipette to expose inner segments for recording.

Patch recording electrodes were pulled on a Narishige (Amityville, NY) PP-830 vertical puller using borosilicate glass pipettes (1.2-mm outer diameter, 0.9-inner diameter with internal filament; World Precision Instruments, Sarasota, FL). Pipettes had tip diameters of 1–2 μm and resistances of 10–15 MΩ. Rod inner segments and cell bodies were identified in flatmount retina and targeted with positive pressure using recording electrodes mounted on Huxley-Wall or motorized micromanipulators (Sutter Instruments). Cones can be distinguished from rods by their larger membrane capacitance and much larger Ca^{2+} currents.

Rod ribbons are surrounded by the glutamate transporters EAAT2 and EAAT5 and glutamate reuptake into rods by these transporters activates a large, anion conductance (Arriza et al., 1997; Eliasof et al., 1998; Grant and Werblin, 1996; Grassmeyer et al., 2019; Hasegawa et al., 2006; Picaud et al., 1995; Schneider et al., 2014). $I_{A(Glu)}$ is activated during glutamate re-uptake but is thermodynamically uncoupled from the transport process (Machtens et al., 2015). To enhance $I_{A(Glu)}$, Cl^- in the patch pipette was replaced with a more permeable anion, thiocyanate (Eliasof and Jahr, 1996). The intracellular pipette solution for these experiments contained (in mM): 120 KSCN, 10 TEA-Cl, 10 HEPES, 1 CaCl2, 1 MgCl2, 0.5 Na-GTP, 5 Mg-ATP, 5 EGTA, 5 phospho-creatine, pH 7.2.

Rod $I_{A(Glu)}$ recordings were performed in whole-cell voltage clamp using an Axopatch 200B amplifier (Molecular Devices) and signals were digitized with a DigiData 1550 (Molecular Devices). Data acquisition and analysis were performed using pClamp 10 software (Molecular Devices). Currents were acquired at 10 kHz and filtered at 2 kHz. Passive membrane resistance was subtracted from $I_{A(Glu)}$ using P/8 subtraction. Membrane capacitance, membrane resistance, and access resistance values for rods using the KSCN solution averaged 3.0 ± 0.4 pF, 3.4± 2.0 GΩ, and 55 ± 9.5 MΩ (n = 9), respectively. Voltages were not corrected for a liquid junction potential of 3.9 mV. Chemical reagents were obtained from Sigma-Aldrich unless otherwise indicated.

Results

Retinas were stained with a knockout-verified primary antibody to Syt9 (green; Synaptic Systems, 105-053; rabbit polyclonal, 1:500) and visualized with Alexa488-conjugated secondary antibody (BD Biosciences, donkey anti-rabbit; 1:200). Labeling was present throughout the retina suggesting Syt9 may be present in many cells (Fig. 1A). Cone terminals were labeled with rhodamine-conjugated peanut agglutinin (PNA, red; Sigma, 10 μg/ml). Antibody labeling was largely abolished in retinas from Syt9 global knockout mice (CMV^{Syt9}, Fig. 1B). We also tested another Syt9 antibody (Neuromab N276A/15) but labeling with this antibody was unchanged in Syt9 global knockout retina.

We used RNAscope techniques to localize Syt9 mRNA in the retina. Consistent with immunohistochemical results, labeling for mRNA was found throughout the retina including photoreceptors (arrows, Fig. 2A), inner retinal neurons (Fig. 2A, B), and an occasional retinal ganglion cell (Fig. 2A, B). Labeling for Syt9 mRNA was particularly prominent in inner segments of photoreceptors and this labeling was eliminated in rod-specific conditional Syt9 knockout mice ($Rod^{Syt9CKO}$, Fig. 2B).

To study the role of Syt9 in synaptic transmission from photoreceptors in shaping bipolar cell light responses, we measured ERGs in vivo from anesthetized mice. Fig. 3A shows representative ERG responses evoked by a high intensity 20 ms flash applied under scotopic conditions to dark-adapted control mice (black trace) and mice in which Syt9 had been globally eliminated (CMV^{Syt9}; red trace). The negative a-wave provides a measure of photoreceptor responses, while the positive b-wave is a measure of second-order ON-type bipolar cell responses. Fig. 3B and C display scotopic a- and b-wave amplitudes, respectively, as a function of increasing flash intensity. Example waveforms for photopic b-waves of light-adapted control (black) and CMV^{Syt9} (red) mice are shown in Fig. 3D. Fig. 3E plots the amplitude of photopic b-wave responses with increasing light intensity. Global elimination of Syt9 increased b-waves under scotopic conditions with higher intensity flashes (Fig. 3C), while scotopic a-waves (Fig. 3B) and photopic b-waves (Fig. 3E) were not significantly different.

Fig. 4 displays measurements from ERGs of control mice and Cone^{Syt9CKO} mice in which Syt9 has been selectively eliminated from cones. Example scotopic ERG waveforms from dark-adapted control and Cone^{Syt9CKO} mice (black and red traces) are shown in Fig. 4A. Scotopic a- and b-wave amplitudes are plotted in Fig. 4B and C, respectively. Eliminating Syt9 from cones did not alter scotopic a- (Fig. 4B) or b-waves (Fig. 4C) significantly. Fig. 4D shows representative photopic ERG waveforms in light-adapted control and Cone^{Syt9CKO} mice. Photopic b-waves from Cone^{Syt9CKO} mice did not differ significantly from control mice (Fig. 4E).

Fig. 5A shows representative ERG responses evoked by a high intensity 20 ms flash applied to dark-adapted control mice and Rod^{Syt9CKO} mice under scotopic conditions in (black and red traces). Scotopic a- and b-wave amplitudes are plotted in Fig. 5B and C, respectively. Rod^{Syt9CKO} mice show diminished b-waves without alterations to the a-wave. Photopic ERG example waveforms are shown in Fig. 5D. Surprisingly, although photopic b-waves were not affected by loss of Syt9 from cones, they were diminished by selective elimination of Syt9 from rods in Rod^{Syt9CKO} mice (Fig. 5E).

We next looked at effects of Syt9 deletion on ERG oscillatory potentials (OPs) that arise from interactions with amacrine cells (Wachtmeister, 1998). Fig. 6 displays measurements of OPs from Syt9 mutant mice under scotopic and photopic conditions. A, A’, and A’’ show representative OPs from CMV^{Syt9}, Cone^{Syt9CKO}, and Rod^{Syt9CKO} mice, respectively. Fig. 6B, B’, and B’’ plot scotopic OPs for the five highest intensity flashes of the scotopic ERG protocol. Photopic OPs are plotted in Fig. 6C, C’, and C’’. The only significant change in OP amplitudes in CMV^{Syt9} mice was an increase in scotopic OPs with the brightest flash intensity (Fig. 6B; t-test with Holm-Sidak correction for multiple comparisons, $P = 0.00142$). Eliminating Syt9 from cones had no effect on OPs under scotopic or photopic conditions (Fig. 34B’, 34C’). However, eliminating Syt9 from rods diminished OP amplitudes under scotopic conditions, with highly significant changes at the three highest flash intensities (Fig. 6B’’; ****$P < 0.00005$), but only small changes to OPs under photopic conditions (Fig. 6C’’).

Reductions in b-wave amplitude without accompanying changes in a-waves are generally evidence of impaired synaptic release from photoreceptors. Given that selective deletion of Syt9 from rods reduced scotopic b-waves at high intensities (Fig. 5), we recorded directly from rods lacking Syt9 (from CMV^{syt9} mice). To assess release, we measured anion currents activated in rods by binding of glutamate to presynaptic EAAT5 glutamate transporters (Grassmeyer et al., 2019). The whole cell pipette solution contained SCN^- as the principal anion to enhance glutamate transporter anion currents ($I_{A(glu)}$). We measured inward currents immediately after termination of depolarizing steps from -70 to -10 for 5, 25, and 500 ms. Fig. 7A shows example waveforms of $I_{A(glu)}$ evoked by 25 ms steps in control (top black trace) and Syt9 KO rods (bottom red trace). Passive capacitative and resistive currents were subtracted using P/6 protocols. We measured both amplitude and charge transfer of $I_{A(glu)}$. As illustrated in Figs. 7B and C, we saw no differences in evoked glutamate release between rods lacking Syt9 and a sample of control rods from C57Bl6J mice with either measurement (Fig. 7). We also analyzed spontaneous release in rods with and without Syt9. The downward transients in the example $I_{A(glu)}$ waveforms in Fig. 7D each represent release of a single synaptic vesicle. Spontaneous release was assessed using 30 s trials with rods held at -70 mV. Spontaneous release of glutamate-filled vesicles persisted in the absence of Syt9 with no change in event frequency (Syt9KO: 0.637 $\pm$ 0.486 v/s, n=10 rods; Control: 0.641 $\pm$ 0.644 v/s, n=13 rods; nested t-test, P=0.85).

Discussion

Global Syt9 deletion showed different effects than selective deletion from rods or cones in mouse retina suggesting involvement of Syt9 at multiple sites in the retina. Global elimination of Syt9 from retina increased the amplitude of scotopic ERG b-wave responses, while deletion from rods alone resulted in decreased scotopic ERG b-waves and OPs. Deletion of Syt9 from cones had no observable effect.

Although deleting Syt9 from cones had no effect, deletion of Syt9 from rods showed effects only at higher flash intensities where cones contribute more significantly. Furthermore, deleting Syt9 from rods reduced photopic b-waves even though photopic responses are driven entirely by cones (Ronning et al., 2018) and eliminating Syt1 from cones is sufficient to abolish photopic ERG responses (Grassmeyer et al., 2019). Rods and cones are coupled to one another by Cx36 gap junctions allowing rod signals to enter cone terminals where they can be transmitted to post-synaptic neurons (Fain and Sampath, 2018). Passage of signals the other way has not been carefully investigated but one possible explanation for these effects is that loss of Syt9 in rods restricts the ability of rods to convey cone signals to downstream neurons. Since release from rods themselves is unimpaired, loss of Syt9 may somehow interfere with gap junction function, perhaps by altering protein trafficking as seen with other Syt isoforms (Wolfes and Dean, 2020).

GABA and glycine are the major inhibitory neurotransmitter in the vertebrate retina (Eggers and Lukasiewicz, 2011) and Syt9 has been shown to modulate GABA release in cultured striatal neurons (Xu et al., 2007). These results led us to consider the possibility that loss of Syt9 might also interfere with GABA and/or glycine release from retinal neurons. Like effects of global deletion of Syt9, blocking $GABA_A$ receptors with bicuculline typically enhances ERG b-waves (Arnarsson and Eysteinsson, 1997; Gottlob et al., 1988; Hirasawa et al., 2021; Vitanova et al., 2001). By contrast, loss of $GABA_C$ receptors and application of $GABA_C$ antagonists have been found to reduce ERG b-waves (Kapousta-Bruneau, 2000; Moller and Eysteinsson, 2003; Wang et al., 2015). This suggests that if Syt9 is modulating GABA release, it is likely to be acting predominantly at synapses possessing $GABA_A$ receptors. Blocking glycine receptors with strychnine can also increase ERG b-waves (Arnarsson and Eysteinsson, 1997; Popova, 2000), but this has not been seen in every preparation (Hirasawa et al., 2021).

The OPs that ride on top of the ERG b-wave are largely due to amacrine cell activity in the inner retina (Wachtmeister, 1998). Loss of Syt9 from rods led to a reduction in scotopic OPs that paralleled

reductions in scotopic b-waves. This suggests that diminished rod input into accompanying loss of Syt9 led in turn to diminished amacrine cell activity further downstream in the retina. Global deletion of Syt9 had smaller effects on OPs, with a small increase in scotopic OPs at the highest intensities. The reduction in OPs produced by eliminating Syt9 from rods might be countered by increases in amacrine cell activity mediated by actions of Syt9 in other cell types. Consistent with a contribution to shaping OPs from diminished GABA release in Syt9 global knockout mice, reducing GABAergic inhibition in $GABA_C$ receptor knockouts can also enhance OPs (McCall et al., 2002). Further studies on the sites and roles of Syt9 in the retina are needed to distinguish these various possibilities.

Funding

Funding provided by NIH grants EY10542 and EY32396 to WT and T32NS105594 to C.S.M. The authors declare no competing financial interests.

Figure legends:

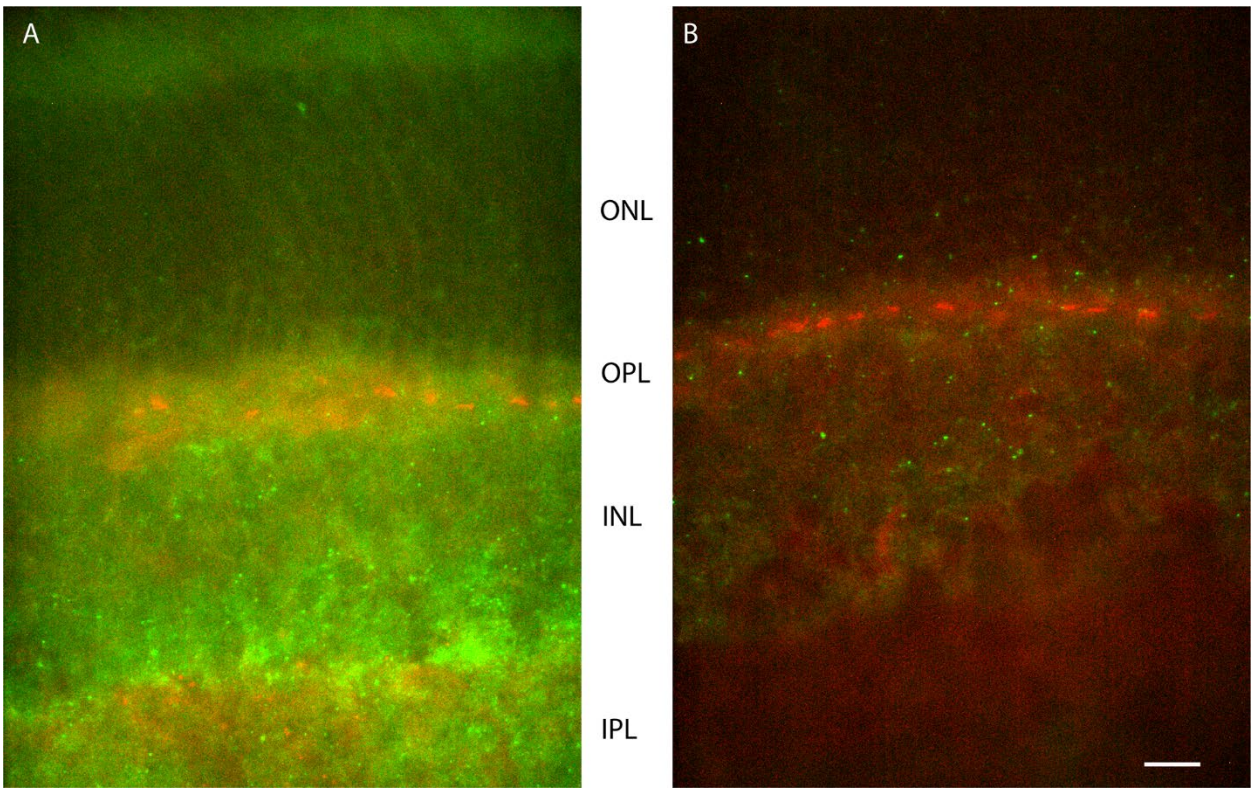

Fig. 1. Immunohistochemical staining suggested the presence of Syt9 throughout the retina. Binding of knockout-verified antibody to Syt9 (Synaptic Systems 105-053) was labeled with Alexa488-conjugated secondary antibody (green; ThermoFisher). Cone terminals were labeled with rhodamine-conjugated peanut agglutinin (PNA; red). (B). Labeling with the Syt9 antibody was largely abolished in retina from a Syt9 global knockout mouse. Single confocal sections. Scale bar: 10 μm.

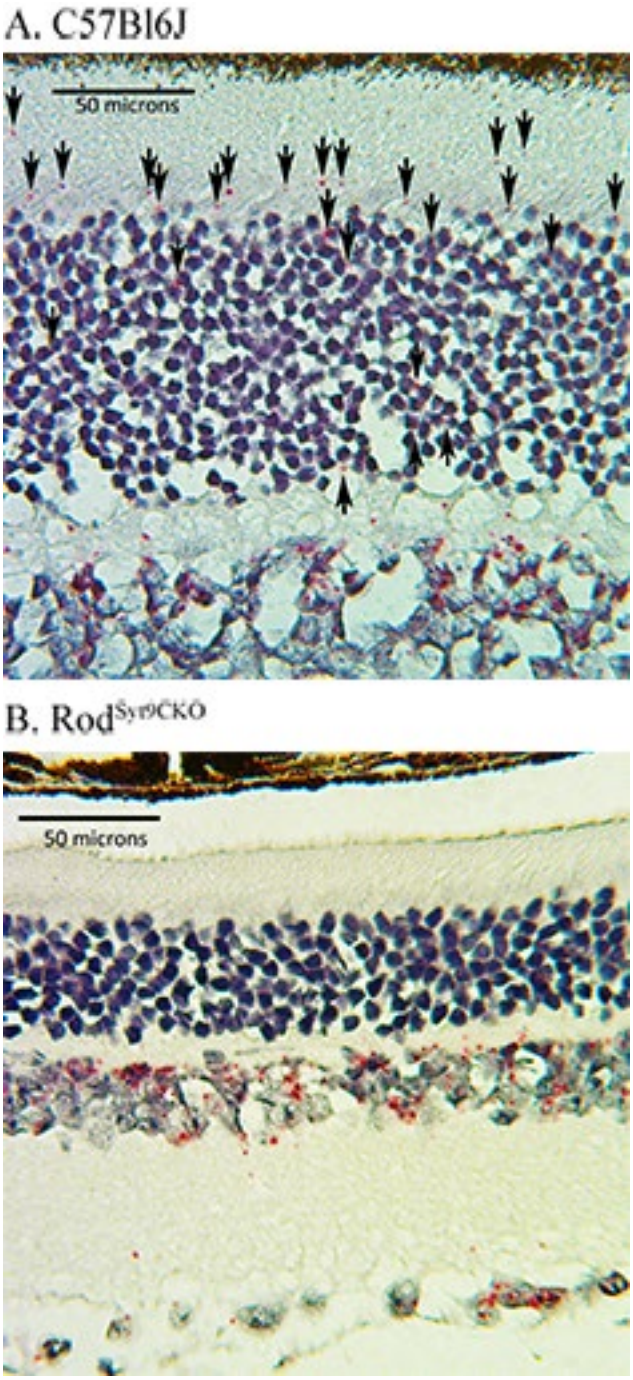

Fig. 2. Syt9 mRNA visualized using RNAscope techniques was present throughout the retina. (A). Syt9 mRNA labeled photoreceptors (arrows), inner retinal neurons, and an occasional retinal ganglion cell. B. Labeling for Syt9 mRNA was eliminated from rods in rod-specific conditional Syt9 knockout mice, but remained in inner retinal neurons and ganglion cells.

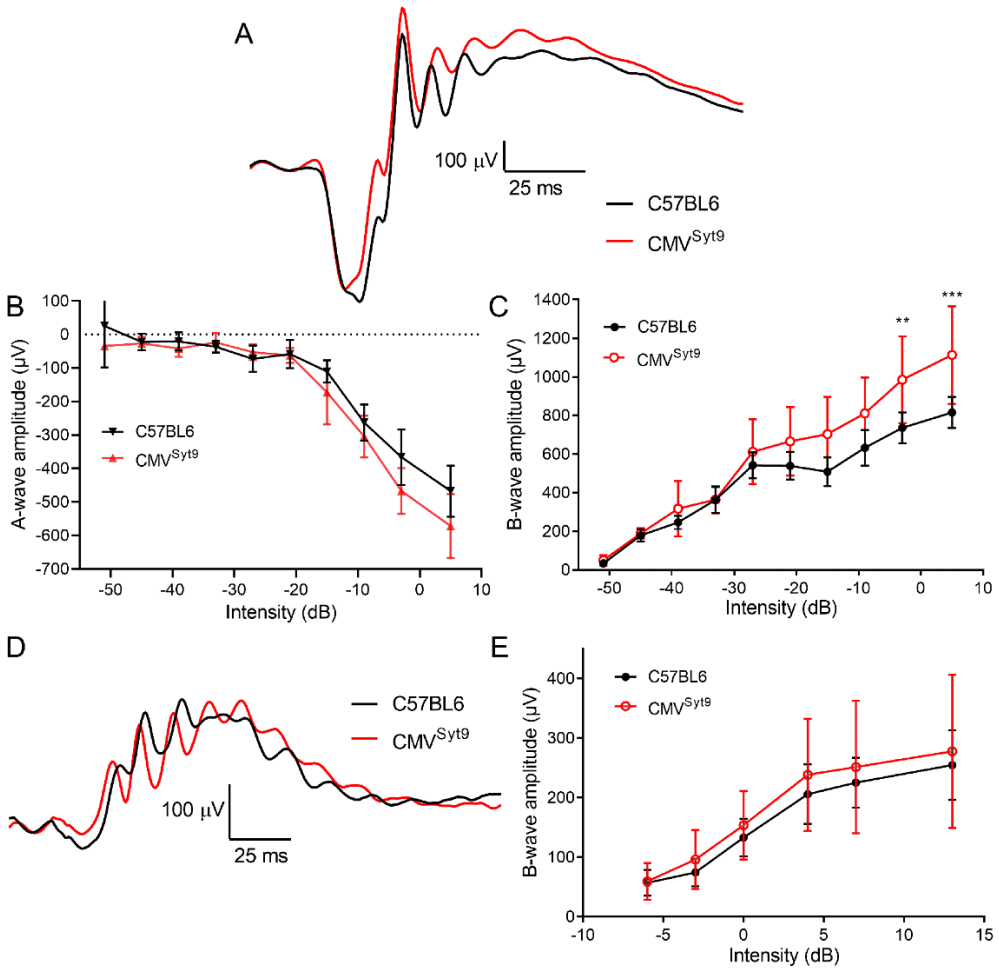

Fig. 3. Global elimination of Syt9 increased scotopic b-wave responses at the highest flash intensities. (A). Representative scotopic ERG waveforms evoked from a high intensity flash (5dB) for control (n=6) and CMV^{Syt9} (n=7) mice are shown in black and red traces, respectively. (B). Scotopic a-wave amplitude as a function of flash intensity. (C). Plot of scotopic b-wave amplitude as a function of intensity. (D). Example photopic waveforms evoked from a high intensity flash (13 dB). (E). Plot of photopic b-wave amplitude as a function of intensity.

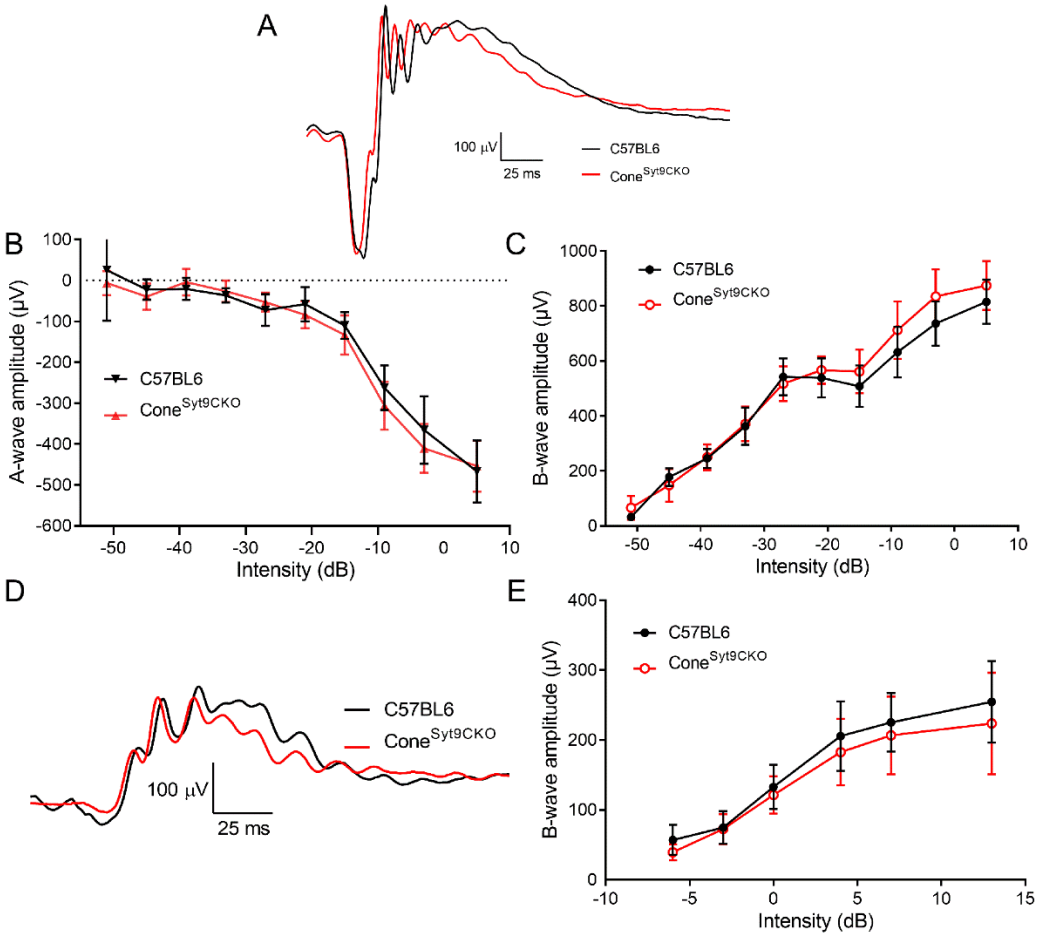

Fig. 4. Elimination of Syt9 selectively from cones had no effect on scotopic or photopic ERG. (A). Representative scotopic ERG waveforms evoked from a high intensity flash (5 dB) for control (n=6) and Cone^{Syt9CKO} (n=7) mice are shown in black and red traces, respectively. (B). Scotopic a-wave amplitude as a function of flash intensity. (C). Plot of scotopic b-wave amplitude as a function of intensity. (D). Example photopic waveforms evoked from a high intensity flash (13 dB). (E). Plot of photopic b-wave amplitude as a function of intensity.

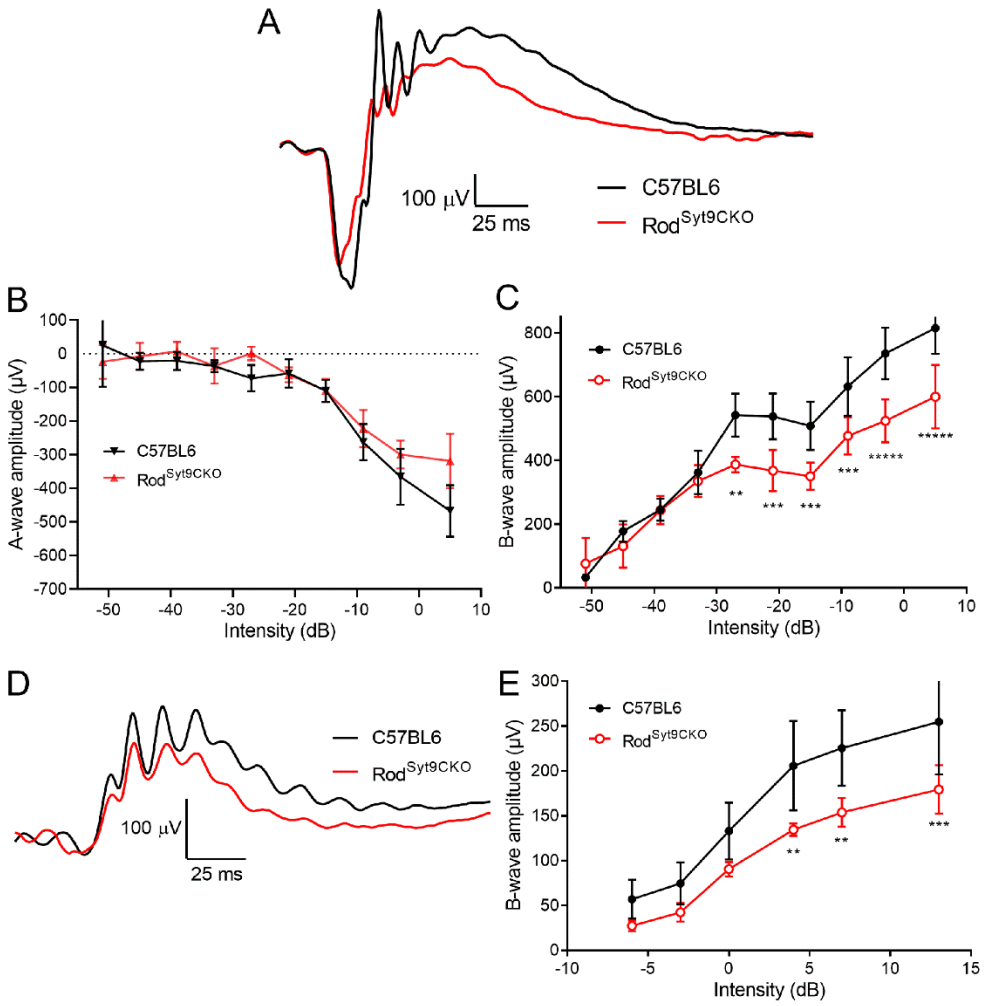

Fig. 5. Elimination of Syt9 selectively from rods decreased scotopic and photopic ERG b-waves. (A). Representative scotopic ERG waveforms (5 dB) for control and Rod^{Syt9CKO} (n=4) mice are shown in black and red traces, respectively. (B). Scotopic a-wave amplitude as a function of flash intensity. (C). Plot of scotopic b-wave amplitude as a function of intensity. (D). Example photopic waveforms evoked from a high intensity flash (13 dB). (E). Plot of photopic b-wave amplitude as a function of flash intensity.

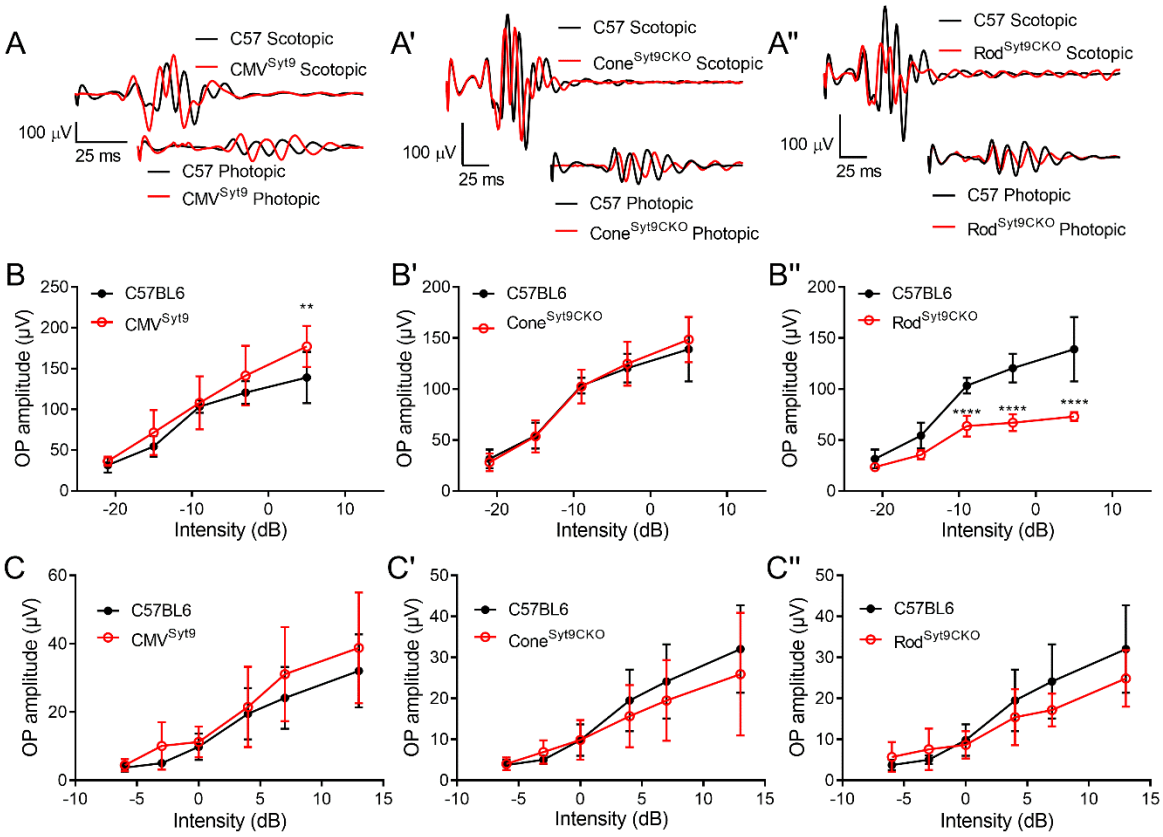

Fig. 6. Effects of Syt9 elimination from the whole retina on ERG oscillatory potentials. (A, A', A''). Scotopic and photopic OPs extracted from representative ERG waveforms (5 dB and 13 dB, respectively) by bandpass filtering to remove frequencies below 70 Hz and above 280 Hz in CMV^{Syt9}, $Cone^{Syt9CKO}$, and $Rod^{Syt9CKO}$ mice, respectively. (B, B', B''). Scotopic OPs in CMV^{Syt9}, $Cone^{Syt9CKO}$, and $Rod^{Syt9CKO}$ mice, respectively.

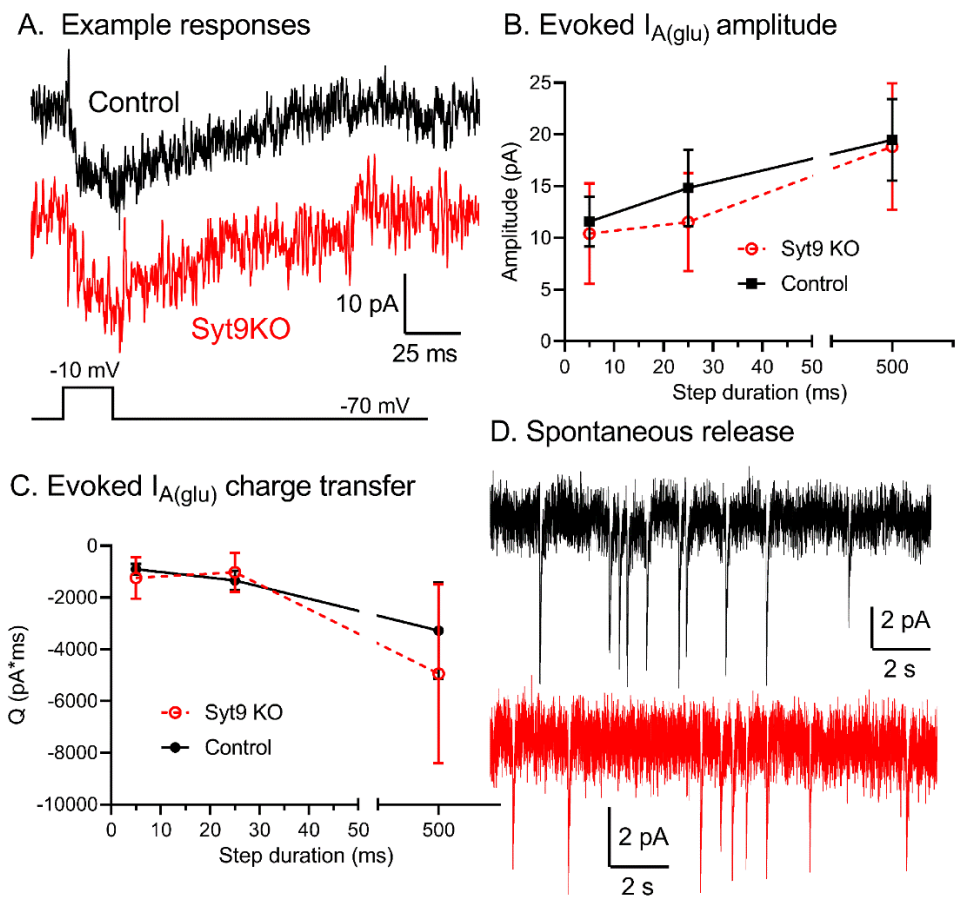

Fig. 7. Whole cell recordings of glutamate transporter anion currents ($I_{A(glu)}$) revealed no significant differences between control and Syt9 KO rods. A. Example $I_{A(glu)}$ recordings from control and Syt9 KO rods evoked by 25 ms steps from -70 to -10 mV. Passive capacitative and resistive currents were subtracted using P/6 protocols. B. $I_{A(glu)}$ amplitude from control (5 ms, n=15; 25 ms, n=16; 500 ms, n=11) and Syt9 KO rods (5 ms, n=34; 25 ms, n=27; 500 ms, n=24). Control data were from (Mesnard et al., 2022). Response amplitude was measured 2 ms after termination of the test step. C. $I_{A(glu)}$ charge transfer from control and Syt9 KO rods. Charge transfer was measured beginning 2 ms after termination of the test step until current recovered to baseline. Baseline was defined as the current level at the end of the 2 s trial. D. Example recordings of spontaneous $I_{A(glu)}$ release events showing release of individual glutamate-filled synaptic vesicles. Rods were held at -70 mV when measuring spontaneous release. Error bars show 95% confidence intervals.

References

Arnarsson, A., and Eysteinsson, T. (1997). The role of GABA in modulating the Xenopus electroretinogram. Vis Neurosci *14*, 1143-1152.

Arriza, J.L., Eliasof, S., Kavanaugh, M.P., and Amara, S.G. (1997). Excitatory amino acid transporter 5, a retinal glutamate transporter coupled to a chloride conductance. Proc Natl Acad Sci U S A *94*, 4155-4160.

Eggers, E.D., and Lukasiewicz, P.D. (2011). Multiple pathways of inhibition shape bipolar cell responses in the retina. Vis Neurosci *28*, 95-108.

Eliasof, S., Arriza, J.L., Leighton, B.H., Kavanaugh, M.P., and Amara, S.G. (1998). Excitatory amino acid transporters of the salamander retina: identification, localization, and function. J Neurosci *18*, 698-712.

Eliasof, S., and Jahr, C.E. (1996). Retinal glial cell glutamate transporter is coupled to an anionic conductance. Proc Natl Acad Sci U S A *93*, 4153-4158.

Fukuda, M. (2006). Distinct developmental expression of synaptotagmin I and IX in the mouse brain. Neuroreport *17*, 179-182.

Fukuda, M., Kowalchyk, J.A., Zhang, X., Martin, T.F., and Mikoshiba, K. (2002). Synaptotagmin IX regulates Ca2+-dependent secretion in PC12 cells. J Biol Chem *277*, 4601-4604.

Fukuda, M., and Sagi-Eisenberg, R. (2008). Confusion in the Nomenclature of Synaptotagmins V and IX: which is which? Calcium Binding Proteins *3*, 1-4.

Geppert, M., Goda, Y., Hammer, R.E., Li, C., Rosahl, T.W., Stevens, C.F., and Sudhof, T.C. (1994). Synaptotagmin I: a major Ca2+ sensor for transmitter release at a central synapse. Cell *79*, 717-727.

Gottlob, I., Wundsch, L., and Tuppy, F.K. (1988). The rabbit electroretinogram: effect of GABA and its antagonists. Vision Res *28*, 203-210.

Grant, G.B., and Werblin, F.S. (1996). A glutamate-elicited chloride current with transporter-like properties in rod photoreceptors of the tiger salamander. Vis Neurosci *13*, 135-144.

Grassmeyer, J.J., Cahill, A.L., Hays, C.L., Barta, C., Quadros, R.M., Gurumurthy, C.B., and Thoreson, W.B. (2019). Ca(2+) sensor synaptotagmin-1 mediates exocytosis in mammalian photoreceptors. Elife *8*.

Hasegawa, J., Obara, T., Tanaka, K., and Tachibana, M. (2006). High-density presynaptic transporters are required for glutamate removal from the first visual synapse. Neuron *50*, 63-74.

Henry, D., Joselevitch, C., Matthews, G.G., and Wollmuth, L.P. (2022). Expression and distribution of synaptotagmin family members in the zebrafish retina. J Comp Neurol *530*, 705-728.

Hirasawa, H., Miwa, N., and Watanabe, S.I. (2021). GABAergic and glycinergic systems regulate ON-OFF electroretinogram by cooperatively modulating cone pathways in the amphibian retina. Eur J Neurosci *53*, 1428-1440.

Hui, E., Bai, J., Wang, P., Sugimori, M., Llinas, R.R., and Chapman, E.R. (2005). Three distinct kinetic groupings of the synaptotagmin family: candidate sensors for rapid and delayed exocytosis. Proc Natl Acad Sci U S A *102*, 5210-5214.

Jin, N., Zhang, Z., Keung, J., Youn, S.B., Ishibashi, M., Tian, L.M., Marshak, D.W., Solessio, E., Umino, Y., Fahrenfort, I.*, et al.* (2020). Molecular and functional architecture of the mouse photoreceptor network. Sci Adv *6*, eaba7232.

Kapousta-Bruneau, N.V. (2000). Opposite effects of GABA(A) and GABA(C) receptor antagonists on the b-wave of ERG recorded from the isolated rat retina. Vision Res *40*, 1653-1665.

Kochubey, O., Babai, N., and Schneggenburger, R. (2016). A Synaptotagmin Isoform Switch during the Development of an Identified CNS Synapse. Neuron *90*, 984-999.

Le, Y.Z., Ash, J.D., Al-Ubaidi, M.R., Chen, Y., Ma, J.X., and Anderson, R.E. (2004). Targeted expression of Cre recombinase to cone photoreceptors in transgenic mice. Mol Vis *10*, 1011-1018.

Li, S., Chen, D., Sauve, Y., McCandless, J., Chen, Y.J., and Chen, C.K. (2005). Rhodopsin-iCre transgenic mouse line for Cre-mediated rod-specific gene targeting. Genesis *41*, 73-80.

Lynch, K.L., and Martin, T.F. (2007). Synaptotagmins I and IX function redundantly in regulated exocytosis but not endocytosis in PC12 cells. J Cell Sci *120*, 617-627.

Machtens, J.P., Kortzak, D., Lansche, C., Leinenweber, A., Kilian, P., Begemann, B., Zachariae, U., Ewers, D., de Groot, B.L., Briones, R.*, et al.* (2015). Mechanisms of anion conduction by coupled glutamate transporters. Cell *160*, 542-553.

McCall, M.A., Lukasiewicz, P.D., Gregg, R.G., and Peachey, N.S. (2002). Elimination of the rho1 subunit abolishes GABA(C) receptor expression and alters visual processing in the mouse retina. J Neurosci *22*, 4163-4174.

Mesnard, C.S., Barta, C.L., Sladek, A.L., Zenisek, D., and Thoreson, W.B. (2022). Eliminating Synaptic Ribbons from Rods and Cones Halves the Releasable Vesicle Pool and Slows Down Replenishment. Int J Mol Sci *23*.

Mittelsteadt, T., Seifert, G., Alvarez-Baron, E., Steinhauser, C., Becker, A.J., and Schoch, S. (2009). Differential mRNA expression patterns of the synaptotagmin gene family in the rodent brain. J Comp Neurol *512*, 514-528.

Moller, A., and Eysteinsson, T. (2003). Modulation of the components of the rat dark-adapted electroretinogram by the three subtypes of GABA receptors. Vis Neurosci *20*, 535-542.

Pang, Z.P., Melicoff, E., Padgett, D., Liu, Y., Teich, A.F., Dickey, B.F., Lin, W., Adachi, R., and Sudhof, T.C. (2006). Synaptotagmin-2 is essential for survival and contributes to Ca2+ triggering of neurotransmitter release in central and neuromuscular synapses. J Neurosci *26*, 13493-13504.

Picaud, S.A., Larsson, H.P., Grant, G.B., Lecar, H., and Werblin, F.S. (1995). Glutamate-gated chloride channel with glutamate-transporter-like properties in cone photoreceptors of the tiger salamander. J Neurophysiol *74*, 1760-1771.

Popova, E. (2000). Glycinergic and GABAergic control of intensity-response function of frog ERG waves under different conditions of light stimulation. Acta Physiol Scand *170*, 225-242.

Quadros, R.M., Miura, H., Harms, D.W., Akatsuka, H., Sato, T., Aida, T., Redder, R., Richardson, G.P., Inagaki, Y., Sakai, D.*, et al.* (2017). Easi-CRISPR: a robust method for one-step generation of mice carrying conditional and insertion alleles using long ssDNA donors and CRISPR ribonucleoproteins. Genome Biol *18*, 92.

Rickman, C., Craxton, M., Osborne, S., and Davletov, B. (2004). Comparative analysis of tandem C2 domains from the mammalian synaptotagmin family. Biochem J *378*, 681-686.

Roper, L.K., Briguglio, J.S., Evans, C.S., Jackson, M.B., and Chapman, E.R. (2015). Sex-specific regulation of follicle-stimulating hormone secretion by synaptotagmin 9. Nat Commun *6*, 8645.

Schneider, N., Cordeiro, S., Machtens, J.P., Braams, S., Rauen, T., and Fahlke, C. (2014). Functional properties of the retinal glutamate transporters GLT-1c and EAAT5. J Biol Chem *289*, 1815-1824.

Seibert, M.J., Evans, C.S., Stanley, K.S., Wu, Z., Briguglio, J.S., and Chapman, E.R. (2022). Synaptotagmin 9 modulates spontaneous neurotransmitter release in striatal neurons by regulating substance P secretion. bioRxiv *10.1101*, 2022.2004.2018.488681v488681.

Vitanova, L., Kupenova, P., Haverkamp, S., Popova, E., Mitova, L., and Wassle, H. (2001). Immunocytochemical and electrophysiological characterization of GABA receptors in the frog and turtle retina. Vision Res *41*, 691-704.

Wachtmeister, L. (1998). Oscillatory potentials in the retina: what do they reveal. Prog Retin Eye Res *17*, 485-521.

Wang, J., Mojumder, D.K., Yan, J., Xie, A., Standaert, R.F., Qian, H., Pepperberg, D.R., and Frishman, L.J. (2015). In vivo electroretinographic studies of the role of GABAC receptors in retinal signal processing. Exp Eye Res *139*, 48-63.

Wolfes, A.C., and Dean, C. (2020). The diversity of synaptotagmin isoforms. Curr Opin Neurobiol *63*, 198-209.

Xu, J., Mashimo, T., and Sudhof, T.C. (2007). Synaptotagmin-1, -2, and -9: Ca(2+) sensors for fast release that specify distinct presynaptic properties in subsets of neurons. Neuron *54*, 567-581.